Int. J. Electrochem. Sci., 13 **(2018)** 9749 – 9758, doi: 10.20964/2018.10.49

International Journal of
ELECTROCHEMICAL
SCIENCE
www.electrochemsci.org

Self-assembled MnO_2/Reduced Graphene Oxide Hybrid Fibers as Electrode Materials for Supercapacitors

Mei Zhang[*], *Yunming Jia and Hongwei Li*[*]

Beijing Key Laboratory of Clothing Materials R & D and Assessment, Beijing Engineering Research Center of Textile Nanofiber, School of Materials Science and Engineering, Beijing Institute of Fashion Technology, Beijing, 100029, China
[*]E-mail: zhangmei7115@163.com; clylihongwei@bift.edu.cn;

Received: 26 May 2018 / *Accepted:* 21 July 2018 / *Published:* 1 September 2018

Hybrid fibers of reduced graphene oxide nanosheets with MnO_2 were fabricated by a facile chemical reduction and self-assembly strategy. FESEM images have shown that MnO_2 rods with diameters of approximately 50-80 nm anchor on the reduced graphene oxide nanosheets as spacers in hybrid fibers, and a certain degree of reduced graphene oxide nanosheets oriented along the main axis of the obtained hybrid fibers has been observed. The electrochemical performance of MnO_2/reduced graphene oxide hybrid fibers (MGFs) as binder-free electrodes is evaluated by using a three-electrode system. The hybrid fibers exhibit a high specific capacitance of 363.2 Fg^{-1} at a constant current density of 200 mAg^{-1}. The improved electrochemical performance can be attributed to the synergistic effect between the MnO_2 and reduced graphene oxide nanosheets in the hybrid fibers and suggests that MGFs with good performance will be a promising electrode material for supercapacitors.

Keywords: MnO_2 rods, Reduced graphene oxide, Hybrid fibers, Flexibility, Supercapacitor.

1. INTRODUCTION

Increasing demands for high-tech electronic products drive rapid advances in developing flexible, lightweight and wearable energy storage systems, which have been utilized in applications ranging from sports products to health monitoring over recent decades [1-5]. Due to their superior power density, long cycle life and safe operation conditions compared with lithium-ion batteries, supercapacitors are highly desirable as a significant class of energy storage devices, and the miniaturization and flexibility of supercapacitors will also become an urgent challenge [6-9]. Flexible and binder-free electrodes play a significant role in future applications for high-performance supercapacitors, which have mainly been fabricated by using amorphous carbon, CNTs or graphene [10-16]. Among these materials, 1D linear graphene fibers with good mechanical flexibility, a

wearable design and high electrical conductivity have been extensively researched [17-20]. Nevertheless, graphene fibers tend to restack into a similar structure with graphite due to the aggregating nature caused by strong π-π interactions, which undermine some excellent characteristics of the individual graphene nanosheets and lead to the relatively low specific capacitance of the electrode material for the supercapacitor [2].

To improve the electrochemical performance of 1D linear graphene fibers, considerable efforts have been devoted to combining graphene fibers with pseudocapacitive materials, such as transition metal oxides (MnO_2, Co_3O_4 and CuO) or conducting polymers (polypyrrole and polyaniline) [1, 21-23]. Among them, MnO_2 has attracted significant attention as an electrode material due to its high theoretical specific capacitance, low cost and environmental friendliness. MnO_2/graphene hybrid fibers have been widely reported as flexible electrodes for supercapacitors [1, 24-25]. The specific capacitance of hybrid fibers is mainly dominated by the pseudocapacitance of the MnO_2 anchored on the graphene fiber surface, and the electric double layer capacitance of the graphene nanosheets is less utilized due to the aggregation of graphene nanosheets in the graphene fibers [1, 26]. Therefore, it is important to develop a simple and low-cost strategy to construct MnO_2/graphene hybrid fibers to increase the utilization rate and combination of MnO_2 and graphene nanosheets in hybrid fibers to achieve good flexibility and excellent electrochemical performance for supercapacitors.

In this paper, MnO_2/reduced graphene oxide hybrid fibers (MGFs) were prepared by a facile low-temperature-induced self-assembly strategy, and the formation process is shown in Fig. 1. The fabrication of MGFs was conducted at 120°C until the hybrid fibers fully formed, and the reduction of graphene oxide to reduced graphene oxide was accompanied by the formation of hybrid fibers, ensuring a certain degree of reduced graphene oxide nanosheets oriented along the main fiber axis. The MGFs deliver a high specific capacitance of 363.2 Fg^{-1} at a current density of 200 mAg^{-1}, which is mainly ascribed to the designed structure and synergistic effect between MnO_2 rods and reduced graphene oxide. The combination of MnO_2 rods and reduced graphene oxide nanosheets can not only mitigate volume changes of MnO_2 rods but also reduce the aggregation of graphene nanosheets in hybrid fibers to improve their electrochemical performance. These hybrid fibers will be potential candidate electrode materials for flexible and bendable supercapacitors.

2. MATERIALS AND METHODS

2.1 Material preparations

All chemicals were of analytical grade and were used as received without further purification. Graphene oxide (GO) suspensions with high concentrations were synthesized by a modified Hummer's method. As shown in Fig. 1, the preparation of MGFs could be divided into three steps: first, 0.1 mol $KMnO_4$ and 0.15 mol $Mn(CH_3COO)_2$ dissolved in 100 ml deionized water was put in an ultrasonic bath for 30 min, and the mixed solution was placed into a 500-mL Teflon-lined autoclave. Then, MnO_2 rods were prepared by a hydrothermal strategy at 90°C for 12 h and washed with deionized water. Second, 6 ml GO solution was diluted to 7 mg ml^{-1} and put in an ultrasonic bath for 30 min and then mixed with the as-prepared MnO_2 rods (2 mg). Third, 0.06 g reducing agent (ascorbic acid) was added

to the mixing solution, and the obtained mixtures were sealed into glass tubes with the specified diameter and kept at 120°C until fibers fully formed to obtain the MnO_2/reduced graphene oxide hybrid fibers (MGFs). The formation of the graphene fibers is mainly due to the capillary forces and surface-tension-induced sheet interactions.

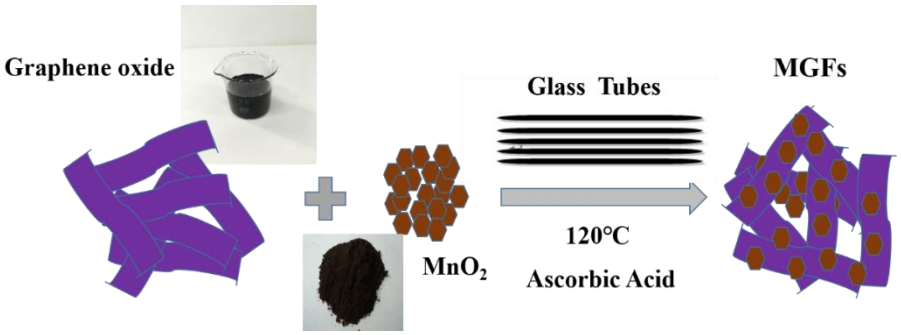

Figure 1. Scheme of MGF synthesis processes.

2.2 Material characterizations

Fourier transform infrared spectra (FTIR, Nicolet Nexus 670) were recorded between 400 cm^{-1} and 4000 cm^{-1} using pressed KBr pellets. The morphologies and structures of the samples were characterized by field emission scanning electron microscopy (FESEM, JEOL JSE-7500F). The other auxiliary information of the products was observed by X-ray diffraction (XRD, X Pert MDP) and X-ray photoelectron spectroscopy (XPS, ESCALAB 250).

2.3 Electrochemical characterization

The electrochemical performance of the as-synthesized MGFs was analyzed in applications of this material as a binder-free and self-supporting electrode material in a three-electrode system using Pt as the counter electrode and Hg/HgO as the reference electrode. Cyclic voltammetry (CV) measurements were carried out at different scan rates (10, 20, 30, 40, 50, 80 and 100 mVs^{-1}) by sweeping the voltage from -0.1 to 0.9 V. The galvanostatic charge-discharge performance was conducted on a LAND instrument at various rates from 0.2 Ag^{-1} to 8.0 Ag^{-1}. The specific capacitance (C, F g^{-1}) of MGFs was calculated by $C = (I \times \Delta t) / (\Delta V \times m)$, where I is the discharge current (A), Δt is the discharge time (s), ΔV is the voltage difference in discharge (V) and m is the mass of the active materials within the electrode (g) [27-28].

3. RESULTS AND DISCUSSION

The FTIR spectra of graphite, GO, MnO_2 and MGFs are shown in Fig. 2. The presence of an oxygen-containing functional group is indicated by the representative peaks of GO, including C-O epoxy groups (1072 cm^{-1} and 1229 cm^{-1}) and C=O stretching of carbonyl and carboxyl groups (1729 cm^{-1}) located at the edges of GO networks [29]. The FTIR spectrum of MnO_2 rods shows a Mn-O

stretching vibration peak at 524 cm^{-1} [30]. However, almost all these characteristic peaks relative to the oxidized groups decreased dramatically in the FTIR spectra of MGFs, and some of them disappeared entirely, which indicates that the oxygen-containing functional groups on the surface and edge of GO are reduced during hybrid fiber formation.

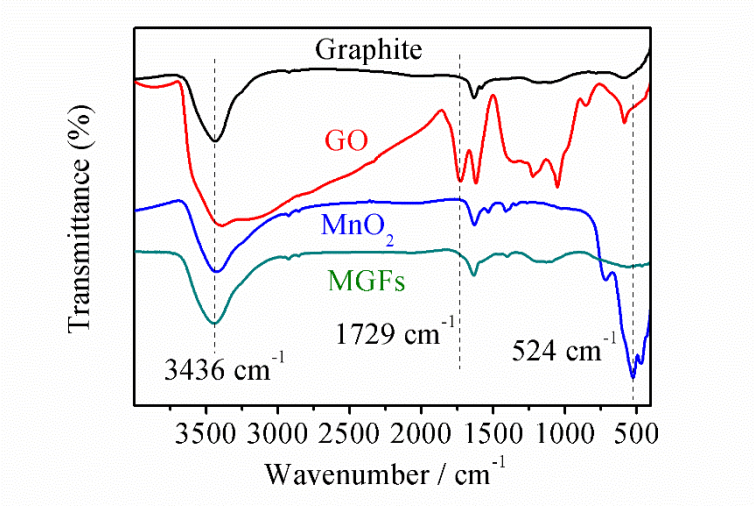

Figure 2. FTIR spectra of graphite, GO, MnO_2 and MGFs.

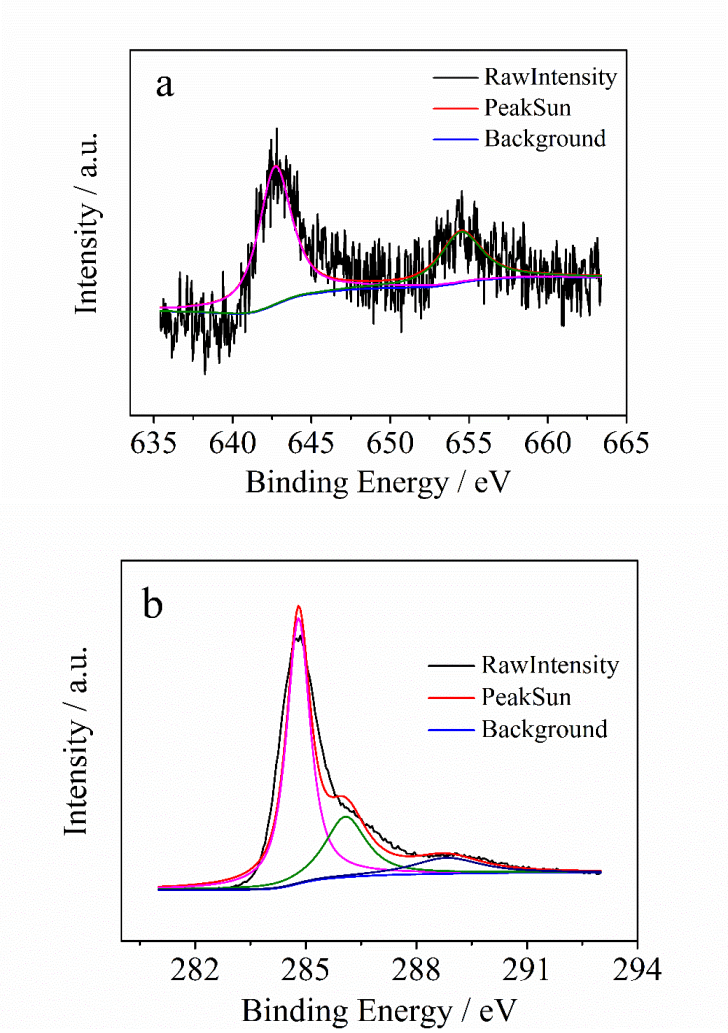

Figure 3. (a) Mn 2p and (b) C 1s XPS spectra of MGFs.

Fig. 3 shows the Mn 2p and C 1s XPS spectra of MGFs. As shown in Fig. 3a, the Mn 2p XPS pattern displays peaks at 642.7 eV and 654.5 eV, which can be attributed to Mn 2p3/2 and Mn 2p1/2 with a spin energy separation of 11.8 eV. The peak values agree well with those reported for MnO_2 [1, 26, 31]. The XPS spectrum of Mn 2p suggests that Mn exists in the 4+ oxidation state, verifying the formation of MnO_2. In Fig. 3b, the MGFs have three typical peaks at 284.8 eV, 286.1 eV and 288.8 eV, corresponding to C=C or C-C, C-O, and C=O or O-C=O, respectively [29]. It is noteworthy that the oxygen-containing functional group peaks at 286.1 eV and 288.8 eV are too weak to detect in the FTIR spectrum, with only a few oxidized groups. The presence of residual oxygen-containing functional groups suggests that there is a C-O-Mn linkage between MnO_2 and reduced graphene oxide, ensuring strong interfacial interactions and structural stability of MGFs.

The MnO_2 rods were prepared by a low-temperature hydrothermal strategy. The XRD pattern of the MnO_2 rods is shown in Fig. 4a. All characteristic peaks at (110), (200), (310), (211), (301), (411), (600) and (521) are in good agreement with the α-MnO_2 crystal (JCPDS 44-0141), and no other impurities are observed [1, 32]. In Fig. 4b-d, the FESEM images are characteristic of MnO_2 rods with different diameters in the range of 50-80 nm and lengths extending from 200 to 500 nm. The rods are constructed with massive MnO_2 nanoparticles, and the average diameter of the nanoparticles is almost 30 nm. The loosely packed MnO_2 nanoparticles can lead to a special structure with a large amount of void spaces, which is beneficial for the contact between active materials and the electrolyte, thus improving the electrochemical performance of the electrode.

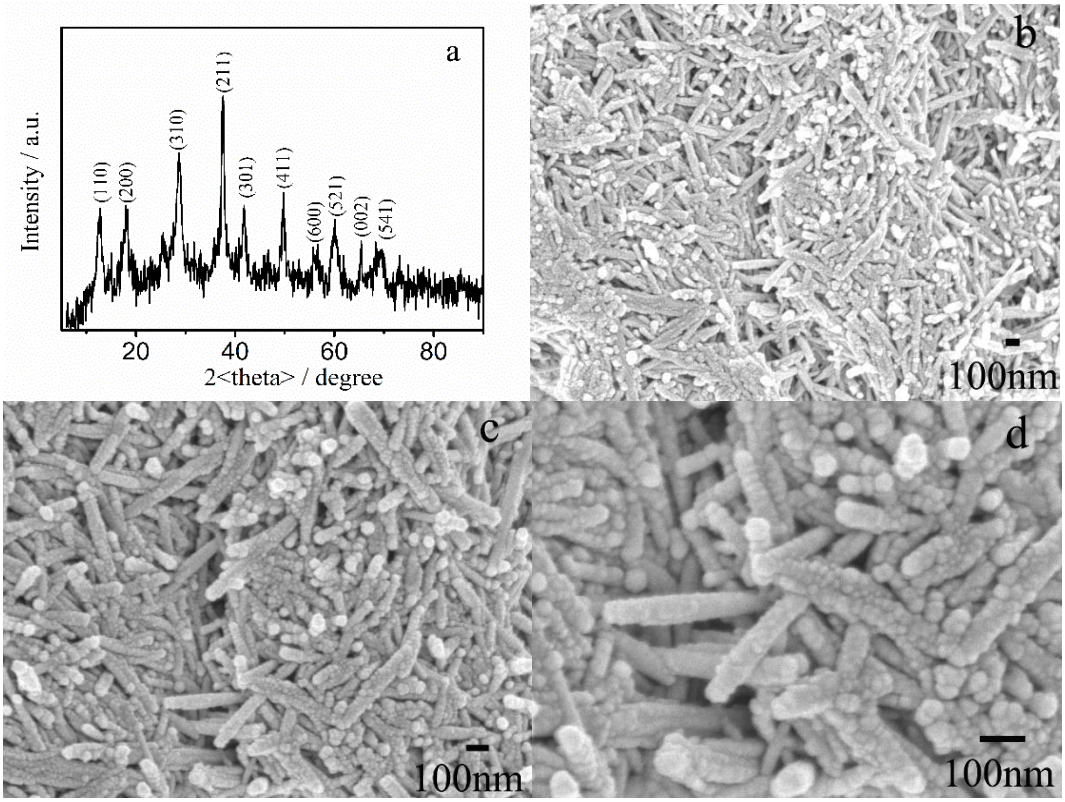

Figure 4. (a) XRD pattern and (b-d) FESEM images of MnO_2 rods.

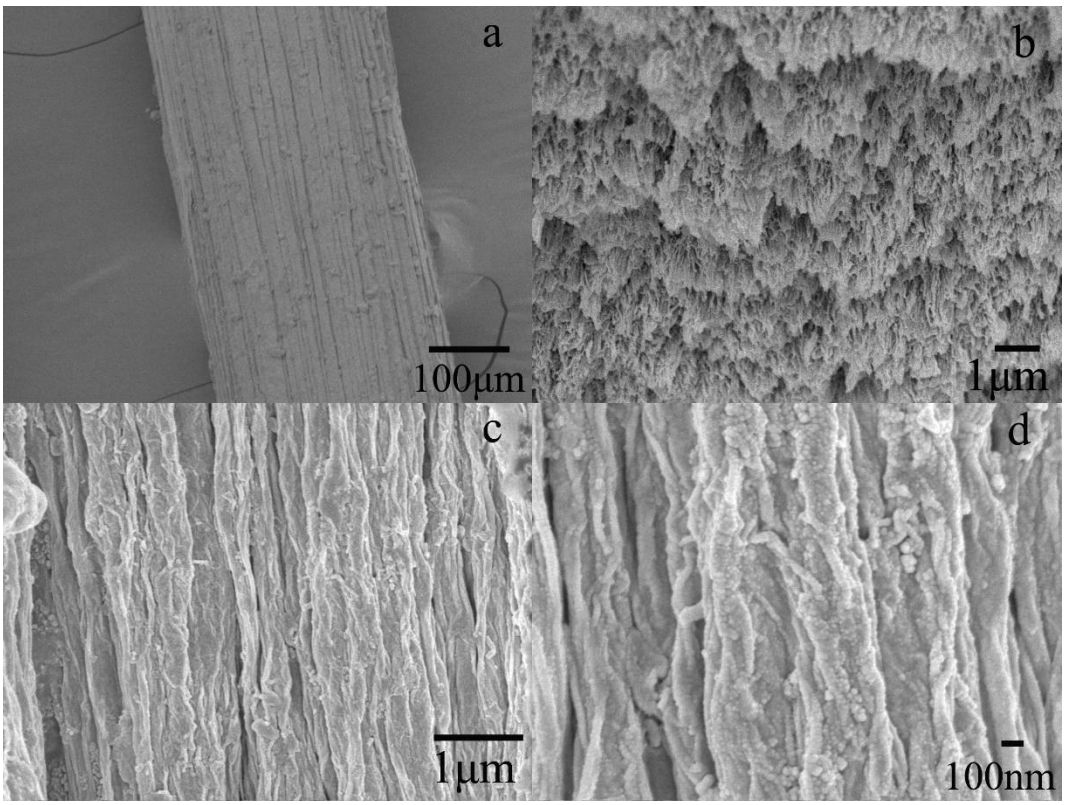

Figure 5. FESEM images of MGFs: (a) low-resolution FESEM image, (b) cross-section morphologies and (c-d) the axial external and inner surface of MGFs.

The morphologies and structures of MnO_2/reduced graphene oxide fibers (MGFs) are characterized by field emission scanning electron microscopy (FESEM), and the experimental results are shown in Fig. 5. The surfaces of the hybrid fibers are not smooth at the microscale, and the diameter is approximately 300 μm (Fig. 5a). The inner cross-section FESEM image of MGFs (Fig. 5b) displays rough and irregular morphologies of the fracture surface. Fig. 5c-d shows the axial external and inner surface morphologies and structures of MGFs. Reduced graphene oxide nanosheets tend to restack into an ordered and porous structure, and the stacked reduced graphene oxide is aligned along the main axis of the fibers. The MnO_2 uniformly disperses between reduced graphene oxide sheets, and the abovementioned combination can effectively reduce the volume change in MnO_2 during the charge-discharge process and prevent the reduced graphene oxide sheets from restacking, thus enhancing the utilization rate of MnO_2 and reduced graphene oxide and increasing the accessible surface area for ion adsorption/desorption, which is beneficial for improving the electrochemical performance of hybrid fibers as binder-free and flexible electrodes for supercapacitors [33-34].

The electrochemical capacitive performance of MGFs was evaluated in 6 M KOH in a three-electrode system. Fig. 6 shows the cyclic voltammogram (CV) curves of the as-synthesized MGFs between -0.1 V and 0.9 V at various sweep rates of 5 mVs^{-1}, 10 mVs^{-1}, 20 mVs^{-1}, 50 mVs^{-1}, 80 mVs^{-1} and 100 mVs^{-1}. With increasing scan rates, the MGFs maintain similar shapes, and the current response shows corresponding increases, revealing good capacitive behavior and kinetic performance of the MGF electrode [26, 35].

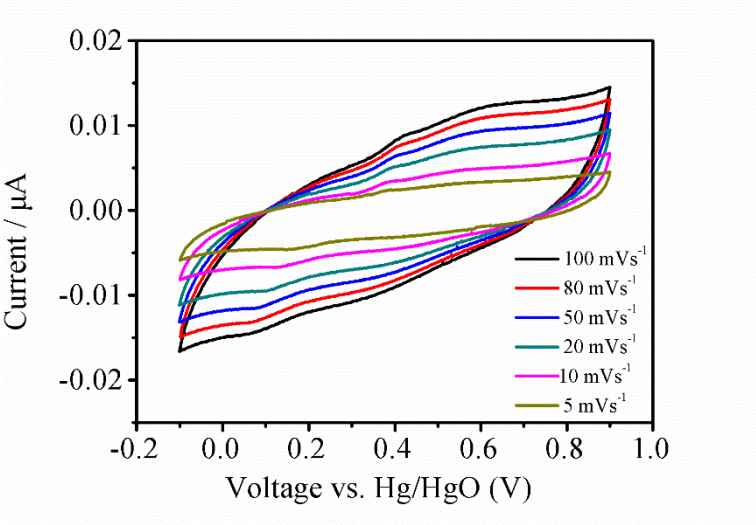

Figure 6. CV curves of MGFs at different sweep rates between 5 mVs^{-1} and 100 mVs^{-1}.

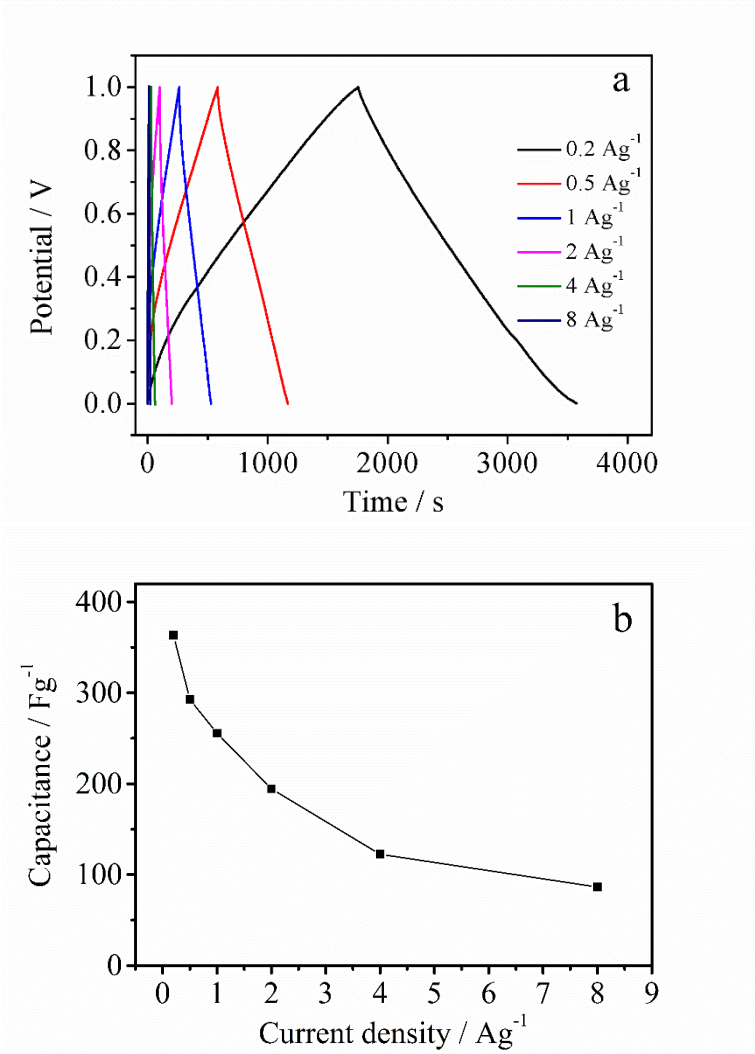

Figure 7. (a) Galvanostatic charge-discharge curves and (b) specific capacitance of MGFs at different current densities of 0.2 Ag^{-1}, 0.5 Ag^{-1}, 1 Ag^{-1}, 2 Ag^{-1}, 4 Ag^{-1} and 8 Ag^{-1}.

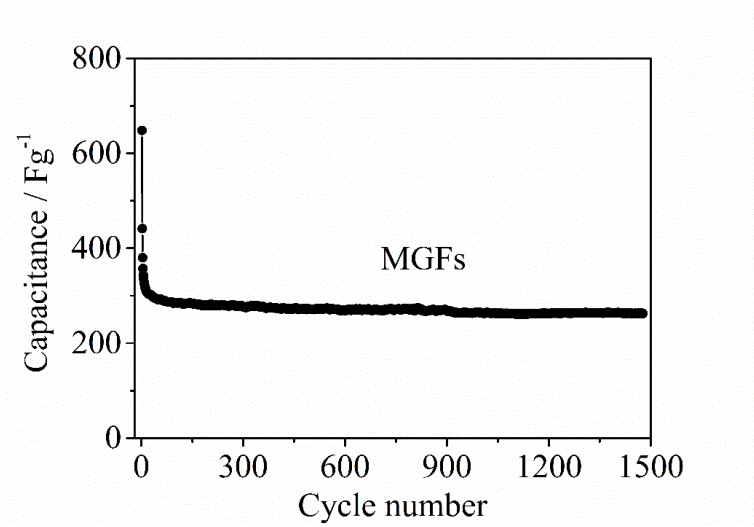

Figure 8. Cycle performance of MGFs at a current density of 0.2 Ag^{-1}.

The results demonstrate the good electrochemical stability of MGFs as electrode materials for supercapacitors. Fig. 7a shows the galvanostatic charge-discharge curves for the MGF electrode at different current densities between 0.2 Ag^{-1} and 8 Ag^{-1}. As the current density increases up to 8 Ag^{-1}, the charge-discharge curves of the MGFs retain their pristine triangle shape, and no obvious distortion is observed. The specific capacitance values are calculated to be 363.2, 292.5, 255.6, 194.4, 122.4, and 86.4 Fg^{-1} at current densities of 0.2, 0.5, 1, 2, 4, and 8 Ag^{-1}, respectively. Fig. 7b displays the rate performance of the MGFs. With increasing charge-discharge current density, the specific capacitance of the MGFs decreases slowly, indicating that MGFs have good rate performance.

The electrochemical stability of MGFs is examined in a 6 M KOH aqueous electrolyte solution through constant charge-discharge at a current density of 0.2 Ag^{-1}, as shown in Fig. 8. The specific capacitance of MGFs is 363.2 Fg^{-1} at a current density of 0.2 Ag^{-1} and remains at 262.8 Fg^{-1} after 1500 charge-discharge cycles. The good specific capacitance is obviously higher than that of graphene fibers reported in our previous report (109.4 Fg^{-1} at 200 mAg^{-1} and maintained at 93.6 Fg^{-1} after 500 cycles) [20]. By combining the electric double layer capacitance of reduced graphene oxide with the pseudocapacitance of MnO_2, the MGFs exhibit good specific capacitance and stable electrochemical performance. This may be attributed to the high theoretical specific capacitance of pseudocapacitive materials and the synergistic effect between MnO_2 and reduced graphene oxide [1, 26]. The incorporation of pseudocapacitive MnO_2 during the formation of hybrid fibers can not only mitigate the aggregation of reduced graphene oxide nanosheets as spacers in hybrid fibers but also reduce the volume change in MnO_2 during the charge-discharge process to increase the utilization rate of the active material and the accessible surface area for ion adsorption/desorption, which is beneficial for improving the electrochemical performance of hybrid fibers as binder-free and flexible electrodes for supercapacitors. According to previous reports, the electrochemical performance of some similar fibers as electrode materials for supercapacitors, such as graphene fibers or MnO_2/graphene hybrid fibers, is listed in table 1 [1, 8, 26, 31, 36-37]. In general, the results show that the MGFs are potential flexible and binder-free electrode materials for supercapacitors.

Table 1. Electrochemical performance of similar fibers used as electrode materials for supercapacitors.

Materials	Preparation method	Electrolyte	Scan rate	Capacitance	Ref
RGO fiber	Wet-spinning, 45% HI, 95°C for 8 h	1 M H_2SO_4	0.2 A g^{-1}	279 F g^{-1}	[8]
RGO fiber	Wet-spinning, 40% HI, 80°C for 6 h.	PVA/H_2SO_4	39.7 mAcm^{-2}	228 mFcm^{-2}	[36]
RGO@3D-G fiber	Glass pipeline, coated with 3D graphene.	PVA/H_2SO_4		25-40 F g^{-1}	[37]
MnO_2/rGO fibers	Wet-spinning	H_3PO_4-PVA	60 mAcm^{-3}	82.6 mFcm^{-2}	[1]
δ-MnO_2/ HRGO fiber	Wet-spinning, δ-MnO_2 coated on fiber surface	1M H_2SO_4	1 Ag^{-1}	245 F g^{-1}	[31]
MnO_2/G/GF	Self-assembly, electrolysis, electrodeposition	H_2SO_4-PVA	Applied current of 2 μA	34-36 F g^{-1}	[26]
MGFs	Self-assembly, ascorbic acid 90°C for 2h and 120°C for 2 h	6 M KOH	0.2 Ag^{-1}	363.2 F g^{-1} 262.8 F g^{-1} after 1500th	This work

4. CONCLUSIONS

In summary, MnO_2/reduced graphene oxide hybrid fibers (MGFs) were prepared by a facile chemical reduction and self-assembly strategy. The MnO_2/reduced graphene oxide hybrid fibers display ordered and porous structures, and the stacked reduced graphene oxide nanosheets are aligned along the main fiber axis. The specific capacitance of MGFs is up to 363.2 Fg^{-1} and remains at 262.8 Fg^{-1} after 1500 charge-discharge cycles at a current density of 0.2 Ag^{-1}, exhibiting a good specific capacitance, rate capability and cycle stability. These results may be attributed to the high specific capacitance of pseudocapacitive materials and the high utilization rate of MnO_2 and reduced graphene oxide. The hybrid fibers are potential candidate materials for use as flexible and binder-free electrode materials for supercapacitors. The method presented in this paper can be extended to induce the assembly of graphene nanosheets and other functional nanophase materials into special structures for various applications.

ACKNOWLEDGMENTS
We acknowledge financial support from the General Program of Science and Technology Development Project of Beijing Municipal Education Commission of China (SQKM201610012002) and the Construction Fund for the High-level Teachers of Beijing Institute of Fashion Technology (BIFTQG201810).

References

1. W. Ma, S. Chen, S. Yang, W. Chen, Y. Cheng, Y. Guo, S. Peng, S. Ramakrishna and M. Zhu, *J. Power Sources,* 306 (2016) 481.
2. S. B. Ni, J. J. Ma, X. H. Lv, X. Yang, L. Zhang, *J. Mater. Chem.* A, 2 (2014) 8995.

3. Q. Yang, Z. Xu, C. Gao, *Journal of Energy Chemistry*, 27 (2018) 6.
4. U. Gulzar, S. Goriparti, E. Miele, T. Li, G. Maidecchi, A. Toma, F. De Angelis, C. Capiglia, *J. Mater. Chem.* A, 4 (2016) 16771.
5. F. Wang, X. Wu, X. Yuan, Z. Liu, Y. Zhang, L. Fu, Y. Zhu, Q. Zhou, Y. Wu and W. Huang, *Chem. Soc. Rev*., 46(2017) 6816.
6. B. Zheng, T. Huang, L. Kou, X. Zhao, K. Gopalsamy and C. Gao, *J. Mater. Chem.* A, 2 (2014) 9736.
7. W. Ma, S. Chen, S. Yang, W. Chen, W. Weng, Y. Cheng, M. Zhu, *Carbon*, 113(2017)151.
8. S. Chen, W. Ma, Y. Cheng, Z. Weng, B. Sun, L. Wang, W. Chen, F. Li, M. Zhu and H. M. Cheng, *Nano Energy*, 15 (2015) 642.
9. L. Li, Z. Wu, S. Yuan and X. Zhang, *Energy Environ. Sci*., 7 (2014) 2101.
10. D. Yu, Q. Qian, L. Wei, W. Jiang, K. Goh, J. Wei, J. Zhang and Y. Chen, *Chem. Soc. Rev*., 44 (2015) 647.
11. T. Chen and L. Dai, *J. Mater. Chem.* A, 2(2014) 10756.
12. X. Cai, C. Zhang, S Zhang, Y. Fang, D. Zou, *J. Mater. Chem.* A, 5(2017) 2444.
13. H. Cheng, Z. Dong, C. Hu, Y. Zhao, Y. Hu, L. Qu, N. Chen and L. Dai, *Nanoscale*, 5 (2013) 3428.
14. K. Guo, N. Yu, Z. Hou, L. Hu, Y. Ma, H. Li, T. Zhai, *J. Mater. Chem.* A, 5(2017) 16.
15. X. Cao, Z. Yin and H. Zhang, *Energy Environ. Sci*., 7 (2014) 1850.
16. S. He and W. Chen, Nanoscale, 7 (2015) 6957.
17. F. Meng, W. Lu, Q. Li, J. H. Byun, Y. Oh and T. W. Chou, *Adv Mater*, 27 (2015) 5113.
18. J. Li, J. Li, L. Li, M. Yu, H. Ma and B. Zhang, *J. Mater. Chem. A*, 2 (2014) 6359.
19. Z. Xu, H. Sun, X. Zhao and C. Gao, *Adv Mater*, 25 (2013) 188.
20. Y. Jia, M. Zhang, H. Li, J. Wang and F. Guan, *Mater. Chem. Phys*., 193 (2017) 35.
21. Y. Zheng, Y. Yang, S. Chen and Q. Yuan, *Cryst. Eng. Comm*., 18 (2016) 4218.
22. X. Zang, M. Zhu, X. Li, X. Li, Z. Zhen, J. Lao, K. Wang, F. Kang, *Nano Energy*, 15 (2015) 83.
23. X. Ding, Y. Zhao, C. Hu, Y. Hu, Z. Dong, N. Chen, Z. Zhang and L. Qu, *J. Mater. Chem.* A, 2 (2014) 12355.
24. M. Huang, F. Li, F. Dong, Y. X. Zhang and L. L. Zhang, *J. Mater. Chem.* A, 3(2015) 21380.
25. M. Huang, L. Wang, S. Chen, L. Kang, Z. Lei, F. Shi, H. Xu and Z. H. Liu, *RSC Advances*, 7(2017)10092.
26. Q. Chen, Y. Meng, C. Hu, Y. Zhao, H. Shao, N. Chen and L. Qu, *J. Power Sources*, 247 (2014) 32.
27. Q. Wu, Y. Xu, Z. Yao, A Liu and G Shi, *ACS Nano*, 4 (2010) 1963.
28. Y. Jin, S. Huang, M. Zhang, M. Jia, *Synth. Met.*, 168 (2013) 58.
29. M. Zhang, Y. Wang and M. Jia, *Electrochimica Acta*, 129 (2014) 425.
30. H E Wang, D Qian, *Mater. Chem. Phys* 109 (2008) 399.
31. J. Zhang, X. Yang, Y. He, Y. Bai, L. Kang, H. Xu, F. Shi, Z. Lei, *J. Mater. Chem*. A, 4(2016) 9088.
32. L. Chen, Z. Song, G. Liu, J. Qiu, C. Yu, J. Qin, L. Ma, F. Tian and W. Liu, *J. Phys. Chem. Solids*, 74 (2013) 360.
33. S. Chen, L. Wang, M. Huang, L. Kang, Z. Lei, H. Xu, F. Shi, Z. Liu, *Electrochim. Acta,* 242(2017)10.
34. M. Abdah, N. Rahman, Y. Sulaiman, *Electrochim. Acta*, 259(2018)466.
35. Q. Zhang, L. Li, Y. Wang, Y. Chen, F. He, S. Gai and P. Yang, *Electrochim. Acta,* 176 (2015) 542.
36. Y Hu, H Cheng, F Zhao, N Chen, L Jiang, Z Feng and L Qu, *Nanoscale,* 6 (2014) 6448-6451.
37. W Cai, T Lai and J Ye. *J. Mater. Chem. A*, 3 (2015) 5060-5066.